JACS
JOURNAL OF THE AMERICAN CHEMICAL SOCIETY

COMMUNICATION

pubs.acs.org/JACS

Monofunctionalization of Protein Nanocages

Feng Li,[†] Yanhua Chen,[†] Huiling Chen,[†] Wei He,[†] Zhi-Ping Zhang,[‡] Xian-En Zhang,*[,‡] and Qiangbin Wang*[,†]

[†]Division of Nanobiomedicine and *i*-Lab, Suzhou Institute of Nano-Tech and Nano-Bionics, Chinese Academy of Sciences, Suzhou 215123 China

[‡]State Key Laboratory of Virology, Wuhan Institute of Virology, Chinese Academy of Sciences, Wuhan, 430071 China

Supporting Information

ABSTRACT: Surface monofunctionalization of protein nanostructures will enable precise topological control over the protein-templated assembly of nanoscale motifs, however, this remains a formidable challenge. Here we demonstrated a novel strategy for this purpose with a protein nanocage, virus-based nanoparticle (VNP) of simian virus 40 as a model system. By simultaneously incorporating a function modality (cysteine) and a purification modality (polyhistidine tag) into the building block (VP1) of VNPs through rational design and genetic engineering, the monofunctionalized cysteine-VNPs are readily obtained through a routine affinity chromatography in virtue of the purification modality of polyhistidine tag, after the coassembly of the functional VP1 and the nonfunctional VP1 at an optimal ratio. This strategy has proved to be highly efficient in constructing monofunctionalized protein nanostructures as highlighted by the monofunctionalized-VNP-guided Au/QD-VNP nanostructures. These nanostructures could be utilized in a wide range of disciplines, including basic biological research, novel nanostructures, and nanodevices fabrication, etc.

Proteins are drawing more and more attention as building blocks and scaffolds to assemble into diverse nanostructures and nanodevices, owing to their intrinsic properties, such as homogeneous size and shape, easy manipulation through rational design/genetic engineering, and facile scaling-up in large quantity.[1−4] In particular, protein nanocages with symmetric hollow structures and configurable self-assembly, like virus-based nanoparticles (VNPs), ferritins, and heat shock proteins, have been extensively investigated as nanoplatforms for synthesis of nanomaterials,[5] organization of nanoparticles,[6,7] fabrication of nanodevices,[8,9] controllable delivery of bioactive molecules,[10,11] etc. Homogenous functionalization of protein nanocage surfaces with genetic or chemical approaches has conferred capabilities, such as targeting and organizing of nanocomponents upon them.[12] Breaking the symmetry and locally functionalizing the surface of a protein nanocage would enable the topological control over the nanoscale assembly guided by protein nanocage scaffolds as well as quantitative investigation of interactions among different entities but remain a technical challenge.

A surface-masking approach for constructing Janus-like protein nanocages has been introduced.[13−15] However, due to the high difficulty in obtaining a masking substrate to expose a very localized part of the protein nanocage surface, functionalization at a specific site (i.e., monofunctionalization) cannot be fully achieved by this approach. It has been reported that protein cages are assembled from different building blocks in a random manner[16,17] and that two kinds of VP1 molecules of polyomavirus A3 fused with different peptides can be coassembled into hybrid VNPs.[18] Therefore, monofunctionalized protein nanocage could be obtained by stoichiometrically coassembling the functional and nonfunctional copies of a building block, however, inevitably mixed with the nonfunctional cages and multifunctional cages. Here we present a novel strategy to monofunctionalize protein nanocages with more precise control and higher yield by coupling the function and the purification modalities in the same building block of a protein cage through rational design and genetic engineering.

The VNPs of simian virus 40 (SV40), which is assembled from 12 VP1 pentamers under appropriate conditions, have been used here to demonstrate this strategy.[19] Based on the structure of VP1 pentamer (PDB ID: 3bwq), the semiexposed alanine 74 on the outside surface (Figure 1, arrow A) was mutated to cysteine to introduce thiol functional groups onto SV40 VNPs, while a tetrahistidine tag was inserted after the surface-exposed histidine 139 for purification purpose (Figure 1, arrow B). The resultant VP1 was named 5hcVP1. The cysteine endows 5hcVP1 with the function of AuNP capturing, while the polyhistidine tag makes it possible to purify the functionalized VNPs by affinity chromatography. The nickel affinities of 5hcVP1 and the wild type VP1 (wtVP1) were assessed using discontinuous imidazole gradients. The wtVP1 can be eluted from the column at 5 mM imidazole, whereas 5hcVP1 strongly binds to the nickel column enduring the elution of 17.5 mM imidazole and can be efficiently eluted with 300 mM imidazole [Figure S1, Supporting Information (SI)]. The significant difference in nickel affinity of the two proteins provides great convenience for separating the functional VNPs from the nonfunctional ones.

To obtain monofunctionalized SV40 VNPs, coassembly of wtVP1 and 5hcVP1 was carried out (Figure 1, step 1). CdSe@ZnS quantum dots (QDs) were introduced into the assembly process to facilitate the postcharacterization of monofunctionalized VNPs, since it has been well established that VP1 can encapsulate QDs, resulting in QD-containing VNPs (QD-VNPs) ca. 24 nm in diameter[20] with 1 QD at the center and 12 surrounding VP1 pentamers arranged in an icosahedral symmetry.[21] During the coassembly, the ratio of 5hcVP1 to wtVP1 determines the probability and purity of the monofunctionalized VNPs that possess 1 5hcVP1 pentamer and 11 wtVP1 pentamers (Figure S2 and Table S1, SI). Accordingly, to obtain monofunctionalized QD-VNPs

Received: August 3, 2011
Published: November 10, 2011

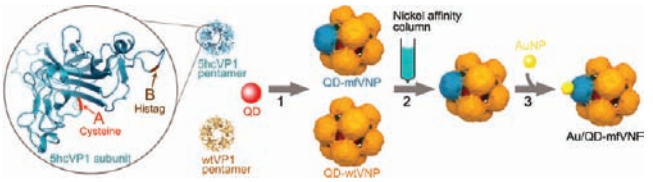

Figure 1. Scheme of the construction of QD-mfVNPs. The enlarged view of the structure of a VP1 unit on the left shows the site of mutagenesis. Arrow A, the alanine 74 that is replaced by cysteine; and arrow B, the histidine 139 after which a tetrahistidine tag is inserted. Step 1, coassembly of wtVP1, 5hcVP1 (the molar ratio of 5hcVP1 to wtVP1 = 1:11) and QDs. Step 2, the QD-mfVNPs are purified from the assembling mixture by nickel affinity chromatography and further purified through sucrose density gradient centrifugation. Step 3, examination of the surface functionality of QD-mfVNPs by AuNP binding assay.

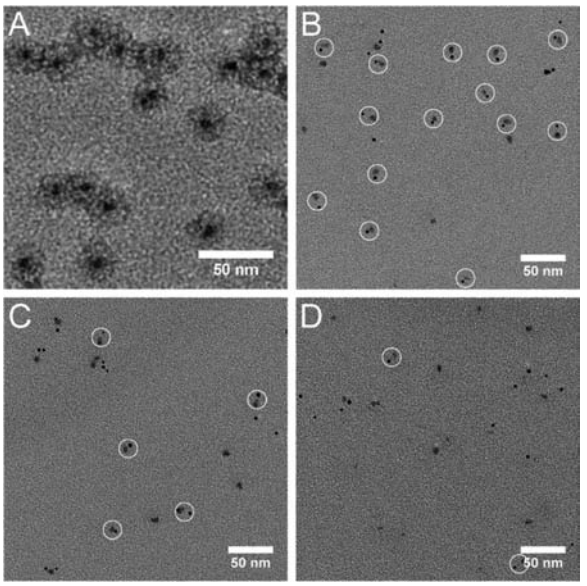

Figure 2. TEM images of QD-mfVNPs (A) and Au/QD-VNP nanostructures (molar ratio of AuNPs to QD-VNPs = 1:1). Au/QD-mfVNPs (B), Au/QD-cVNPs (C), and Au/QD-wtVNPs (D). Circles indicate one AuNP-one QD-VNP nanostructures.

(QD-mfVNPs) at the highest yield, 5hcVP1 and wtVP1 were mixed at a molar ratio of 1:11. The mixture was loaded into a nickel affinity column which was subsequently washed with 5 and 17.5 mM imidazole to eliminate any QD-VNPs assembled from mere wtVP1 (QD-wtVNPs). The QD-mfVNPs were eluted from the column with 300 mM imidazole (Figure 1, step 2). There might be free 5hcVP1 pentamers in the fraction eluted with 300 mM imidazole, so the fraction was then subjected to sucrose density gradient centrifugation to further purify the QD-mfVNPs (Figure S3, SI). The transmission electron microscopy (TEM) image of the as-prepared QD-mfVNPs shows structural integrity with one QD inside (Figure 2A).

As predesigned, the QD-mfVNPs possess one cysteine-functionalized VP1 pentamer among the 12 VP1 pentamers, therefore, the AuNP binding assay was used to test the monofunction characteristic of QD-mfVNPs (Figure 1, step 3). We previously developed an SV40 VNP-based strategy for constructing discrete three-dimensional hybrid ensembles of nanoparticles.[21]

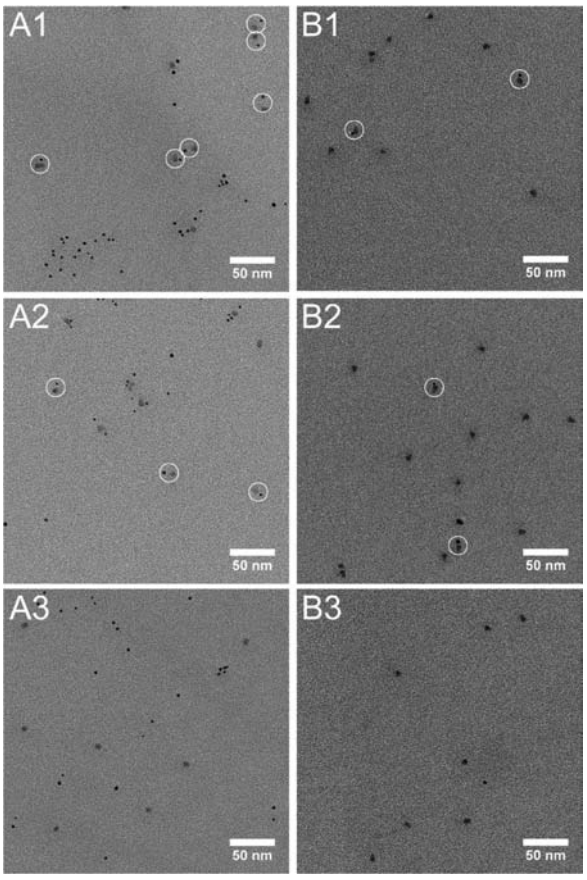

Figure 3. TEM images of Au/QD-VNP nanostructures at different molar ratios of AuNPs to QD-VNPs. A1−A3: Au/QD-mfVNPs, Au/QD-cVNPs, and Au/QD-wtVNPs at a molar ratio of 3:1, respectively. B1−B3: Au/QD-mfVNPs, Au/QD-cVNPs, and Au/QD-wtVNPs at a molar ratio of 1:5, respectively. Circles indicate one AuNP-one QD-VNP nanostructures.

AuNPs bind to the thiol groups on the surface of QD-cVNPs (made of 12 pentamers of a VP1 mutant Ala74Cys, that is, all the VP1 pentamers have 5 cysteines exposed outside), and the number of AuNPs on QD-cVNPs is tuned by adjusting the ratio of AuNPs to QD-cVNPs.[21] On the surface of QD-mfVNPs, one 5hcVP1 provides five thiol groups that are distributed on a virtual circle of 4 nm in diameter and can capture one AuNP with a similar or larger diameter. AuNPs with an average size of 4.2 nm capped by dihydrolipoic acid (DHLA) were allowed to assemble onto QD-mfVNPs at a molar ratio of 1:1. Binding of AuNPs to QD-cVNPs and QD-wtVNPs was also performed in parallel as references.

Figure 2 depicts typical TEM images of different Au/QD-VNP nanostructures with a stoichiometric ratio of AuNPs to QD-VNPs, in which the lower contrast dots represent the QD-VNPs and the higher contrast dots denote the AuNPs. Since the shell thickness of QD-VNPs is ca. 7 nm,[22] AuNP-QD pairs with interparticle distance within 7 nm were counted as target Au/QD-VNP ensembles. In the Au/QD-mfVNP samples, one AuNP-one QD-VNP nanostructures are dominantly observed (Figures 2B and S4, SI). Differently, in the Au/QD-cVNP samples, objects containing one QD-VNP with variable numbers (1−3) of AuNPs are all observed (Figures 2C and S5, SI). However, in the Au/QD-wtVNP samples, free QDs and AuNPs

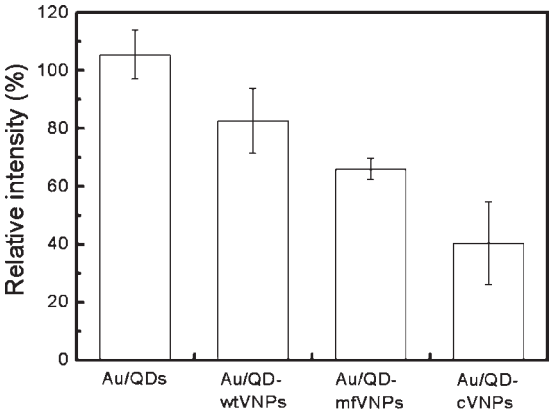

Figure 4. PL of different Au/QD-VNP nanostructures (molar ratio of AuNPs to QD-VNPs = 1:1). Au/QDs stands for the mixture of AuNPs and QDs at 1:1 ratio. The relative intensity stands for the ratio of the PL intensity of Au/QD-VNPs to that of the corresponding QD-VNPs without AuNPs. In all the samples, the concentrations of AuNPs and QDs are kept constant.

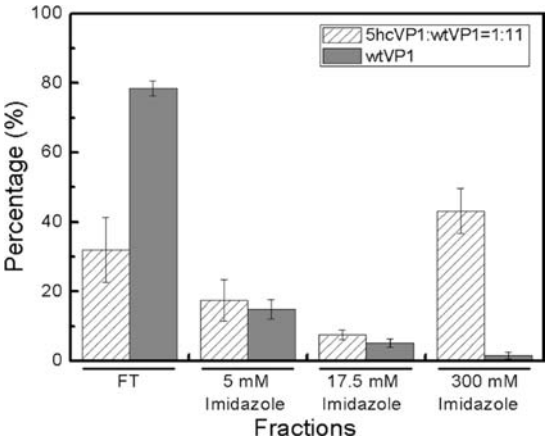

Figure 5. Distribution of VP1 in the purification of QD-mfVNPs. FT: flow-through.

are frequently observed (Figures 2D and S6, SI). Meanwhile, some random Au/QD-wtVNP ensembles are also observed, which is likely due to nonspecific binding of AuNPs to QD-wtVNPs or to aggregation of particles during TEM sampling.

Based on the statistic analysis of ~100 assembles, 92% of one AuNP-one QD-VNP structures were obtained using our designed mfVNP as template with a stoichiometric ratio of AuNPs to QD-mfVNPs, which illustrated the success of our strategy in monofunctionalizing the protein nanocages. Binding of AuNPs to QD-VNPs at higher and lower ratios was further performed to testify the monofunctionalization of VNPs. At a higher ratio (3:1), one AuNP-one QD-VNP nanostructures are still dominantly observed in the Au/QD-mfVNP samples (Figures 3A1 and S7, SI). In contrast, ensembles with one QD-VNP and a few (1−4) AuNPs are formed in the Au/QD-cVNP samples (Figures 3A2 and S8, SI). As controls, in the Au/QD-wtVNP samples, most of the QD-VNPs and AuNPs are distributed discretely on the carbon film without forming Au/QD ensembles (Figures 3A3 and S9, SI). At a lower ratio (1:5), one AuNP-one QD-VNP nanostructures are less observed in samples guided by mfVNPs and cVNPs (Figures 3B1, 3B2, S10, and S11, SI) and not formed with wtVNPs as templates (Figures 3B3 and S12, SI). It is notable that bridging structures like QD-VNP-AuNP-QD-VNP were rarely found, which can be explained as follows. The ζ potentials of QD-mfVNPs and QD-cVNPs were determined to be ca. −30 mV under the AuNP binding condition (pH = 8). It is very difficult for a AuNP with a diameter of 4.2 nm to simultaneously bind to two 24 nm-sized QD-mfVNPs or QD-cVNPs due to the repulsion and steric hindrance between QD-VNPs. These results provide extra evidence for the monofunctionalization of SV40 VNPs.

In addition to the TEM characterization, the photoluminescence (PL) intensities of different Au/QD-VNP nanostructures can also provide evidence of the formation of Au/QD-mfVNP nanostructures since the PL intensity of QDs is closely related to the status of the surrounding AuNPs onto the VNP surface.[21] Figure 4 shows a summary of the PL intensities of different Au/QD-VNP nanostructures at the 1:1 ratio. The PL intensity of the Au/QD-wtVNPs decreased to around 83% of the blank, which resulted from the weak quenching of nonspecific binding of AuNPs onto QD-wtVNPs. The PL intensity of Au/QD-mfVNPs was lowered to ca. 66%, while that of Au/QD-cVNPs was dropped to ca. 40% of the blank. Such difference agrees with that QD-cVNPs have much more cysteines exposed on surface and are thus more powerful in capturing AuNPs in comparison with QD-mfVNPs, as shown in TEM images (Figure 2). These results further illustrated that our strategy works for high-yield fabrication of monofunctional VNPs which consist of a single functional pentamer (5hcVP1) and 11 nonfunctional pentamers (wtVP1).

As reported that two kinds of VP1 molecules of polyomavirus A3 fused with different peptides can be coassembled into hybrid VNPs,[18] our analysis of the distribution of total VP1 (including wtVP1 and 5hcVP1) also confirms the occurrence of coassembling of 5hcVP1 and wtVP1 into VNP. Figure 5 shows the distribution of VP1 during the purification of QD-mfVNPs, compared with QD-wtVNPs. According to the nickel affinity of 5hcVP1 and wtVP1 (Figure S1, SI), at 17.5 mM of imidazole, most of 5hcVP1 are immobilized on the column because of the strong binding of the introduced polyhistidine tag, but wtVP1 is nearly cleared away. Therefore, the fractions of flow-through (FT), 5 and 17.5 mM imidazole correspond to wtVP1 pentamers and QD-wtVNPs, and the fraction of 300 mM imidazole corresponds to 5hcVP1 pentamers and QD-mfVNPs. For the assembly of wtVP1, ca. 80% of VP1 flowed through the column, and most of the VP1 (>98%) had been removed from the column after the wash of 17.5 mM imidazole. In contrast, in the case of 1:11 coassembly of 5hcVP1 and wtVP1, only ca. 30% of VP1 flowed through the column. After washing with 5 and 17.5 mM imidazole, more than 40% of VP1 was eluted with 300 mM imidazole, much higher than 8.3%, the percentage of 5hcVP1 in the total VP1 initially added, which is consistent with that of wtVP1 immobilized onto the column in virtue of 5hcVP1 after the coassembly of the two kinds of VP1. The results also suggest that the purification and function modalities involved amino acids are exposed on the surface of the assembled cages as predesigned.

In order to further characterize the nature of QD-mfVNPs, the content of 5hcVP1 was quantified. QD-mfVNPs were dissociated under denaturing conditions (see Experimental Section, SI). After confirming that the nickel affinity of 5hcVP1 was not affected by the denaturing conditions or in the presence of QDs (Figure S13, SI), 5hcVP1 and wtVP1 were separated using nickel affinity chromatography and quantified by SDS-PAGE/

densitometry (Figure S14, SI). The 5hcVP1 was found to constitute ca. 9% of the total protein in QD-mfVNPs, approximating to the predicted percentage (8.3% = 1/12 × 100%) of 5hcVP1 in ideally monofunctionalized VNPs. This indicates that the monofunctionalized cages consisting of 1 5hcVP1 and 11 wtVP1 pentamers dominate in the as-prepared QD-mfVNPs. The high efficiency in obtaining monofunctionalized VNPs is attributed to: (1) coassembly of 5hcVP1 and wtVP1 at an optimal ratio and (2) further screening of the QD-mfVNPs in virtue of the nickel affinity difference of VNPs containing different copies of 5hcVP1 (Figure S15, SI).

In summary, we have demonstrated a highly efficient strategy for monofunctionalizing SV40 VNPs through rational design and genetic manipulation of their building block, VP1. The VP1 pentamer is engineered for simultaneous introduction of surface-exposed cysteines and polyhistidine tags. The mfVNPs is assembled by incorporating the functional VP1 pentamer and its nonfunctional counterpart at an optimal ratio. The polyhistidine tags make it possible to purify the monofunctionalized protein nanocages through nickel affinity chromatography. AuNP binding assay illustrates the monofunctionality nature of the as-obtained mfVNPs and the capability of mfVNP in organizing heterogeneous nanostructure composed of one QD and one AuNP. We expect that this novel strategy can be generalized to other proteins and nanomotifs and readily used for monofunctionalization of inorganic NPs, deliberate design, and construction of complex nanoarchitectures, single-particle tracking, quantitative investigation of host−guest interaction as well as preorientated imaging, targeting, and drug delivery, etc.

■ ASSOCIATED CONTENT

Supporting Information. Experimental section and additional images of TEM, SDS-PAGE, and SDGC tube. This material is available free of charge via the Internet at http://pubs.acs.org.

■ AUTHOR INFORMATION

Corresponding Author
qbwang2008@sinano.ac.cn; x.zhang@wh.iov.cn

■ ACKNOWLEDGMENT

F.L. acknowledges funding by NSFC (no. 31040032), JSNSF (no. BK2010260), and China Postdoctoral Science Foundation (no. 20110491460); Q.W. acknowledges funding by the "Bairen Ji Hua" program and "Strategic Priority Research Program" (no. XDA01030200) from CAS, MOST (no. 2011CB965004), NSFC (no. 91023038), and CAS/SAFEA International Partnership Program for Creative Research Teams. Z.Z. thanks funding by MOST (no. 2011CB933600). The authors thank Peidong Yang at UC Berkeley for helpful discussions.

■ REFERENCES

(1) Olasagasti, F.; Lieberman, K. R.; Benner, S.; Cherf, G. M.; Dahl, J. M.; Deamer, D. W.; Akeson, M. *Nat. Nanotechnol.* **2010**, *5*, 798.
(2) de la Rica, R.; Matsui, H. *Chem. Soc. Rev.* **2010**, *39*, 3499.
(3) Knowles, T. P.; Oppenheim, T. W.; Buell, A. K.; Chirgadze, D. Y.; Welland, M. E. *Nat. Nanotechnol.* **2010**, *5*, 204.
(4) Ballister, E. R.; Lai, A. H.; Zuckermann, R. N.; Cheng, Y.; Mougous, J. D. *Proc. Natl. Acad. Sci. U.S.A.* **2008**, *105*, 3733.
(5) Douglas, T.; Young, M. *Nature* **1998**, *393*, 152.
(6) Wang, Q.; Lin, T. W.; Tang, L.; Johnson, J. E.; Finn, M. G. *Angew. Chem., Int. Ed.* **2002**, *41*, 459.
(7) Blum, A. S.; Soto, C. M.; Wilson, C. D.; Cole, J. D.; Kim, M.; Gnade, B.; Chatterji, A.; Ochoa, W. F.; Lin, T. W.; Johnson, J. E.; Ratna, B. R. *Nano Lett.* **2004**, *4*, 867.
(8) Lin, X.; Xie, J.; Niu, G.; Zhang, F.; Gao, H.; Yang, M.; Quan, Q.; Aronova, M. A.; Zhang, G.; Lee, S.; Leapman, R.; Chen, X. *Nano Lett.* **2011**, *11*, 814.
(9) Tseng, R. J.; Tsai, C.; Ma, L.; Ouyang, J.; Ozkan, C. S.; Yang, Y. *Nat. Nanotechnol.* **2006**, *1*, 72.
(10) O'Neil, A.; Reichhardt, C.; Johnson, B.; Prevelige, P. E.; Douglas, T. *Angew. Chem., Int. Ed.* **2011**, *50*, 7425.
(11) Tong, G. J.; Hsiao, S. C.; Carrico, Z. M.; Francis, M. B. *J. Am. Chem. Soc.* **2009**, *131*, 11174.
(12) Soto, C. M.; Ratna, B. R. *Curr. Opin. Biotechnol.* **2010**, *21*, 426.
(13) Klem, M. T.; Willits, D.; Young, M.; Douglas, T. *J. Am. Chem. Soc.* **2003**, *125*, 10806.
(14) Suci, P. A.; Kang, S.; Young, M.; Douglas, T. *J. Am. Chem. Soc.* **2009**, *131*, 9164.
(15) Kang, S.; Suci, P. A.; Broomell, C. C.; Iwahori, K.; Kobayashi, M.; Yamashita, I.; Young, M.; Douglas, T. *Nano Lett.* **2009**, *9*, 2360.
(16) Gillitzer, E.; Suci, P.; Young, M.; Douglas, T. *Small* **2006**, *2*, 962.
(17) Kang, S.; Oltrogge, L. M.; Broomell, C. C.; Liepold, L. O.; Prevelige, P. E.; Young, M.; Douglas, T. *J. Am. Chem. Soc.* **2008**, *130*, 16527.
(18) Shin, Y. C.; Folk, W. R. *J. Virol.* **2003**, *77*, 11491.
(19) Kanesashi, S. N.; Ishizu, K.; Kawano, M. A.; Han, S. I.; Tomita, S.; Watanabe, H.; Kataoka, K.; Handa, H. *J. Gen. Virol.* **2003**, *84*, 1899.
(20) Li, F.; Zhang, Z. P.; Peng, J.; Cui, Z. Q.; Pang, D. W.; Li, K.; Wei, H. P.; Zhou, Y. F.; Wen, J. K.; Zhang, X. E. *Small* **2009**, *5*, 718.
(21) Li, F.; Gao, D.; Zhai, X.; Chen, Y.; Fu, T.; Wu, D.; Zhang, Z. P.; Zhang, X. E.; Wang, Q. *Angew. Chem., Int. Ed.* **2011**, *50*, 4202.
(22) Liddington, R. C.; Yan, Y.; Moulai, J.; Sahli, R.; Benjamin, T. L.; Harrison, S. C. *Nature* **1991**, *354*, 278.